

## MIT Open Access Articles

*Bimodal rheotactic behavior reflects flagellar beat asymmetry in human sperm cells*

The MIT Faculty has made this article openly available. **Please share** how this access benefits you. Your story matters.

**Citation:** Bukatin, Anton et al. "Bimodal Rheotactic Behavior Reflects Flagellar Beat Asymmetry in Human Sperm Cells." *Proceedings of the National Academy of Sciences* 112.52 (2015): 15904–15909. © 2017 National Academy of Sciences

**As Published:** <http://dx.doi.org/10.1073/pnas.1515159112>

**Publisher:** National Academy of Sciences (U.S.)

**Persistent URL:** <http://hdl.handle.net/1721.1/110648>

**Version:** Final published version: final published article, as it appeared in a journal, conference proceedings, or other formally published context

**Terms of Use:** Article is made available in accordance with the publisher's policy and may be subject to US copyright law. Please refer to the publisher's site for terms of use.



# Bimodal rheotactic behavior reflects flagellar beat asymmetry in human sperm cells

Anton Bukatin<sup>a,b,1</sup>, Igor Kukhtevich<sup>b,c,1</sup>, Norbert Stoop<sup>d,1</sup>, Jörn Dunkel<sup>d,2</sup>, and Vasily Kantsler<sup>e</sup>

<sup>a</sup>St. Petersburg Academic University, St. Petersburg 194021, Russia; <sup>b</sup>Institute for Analytical Instrumentation of the Russian Academy of Sciences, St. Petersburg 198095, Russia; <sup>c</sup>ITMO University, St. Petersburg 197101, Russia; <sup>d</sup>Department of Mathematics, Massachusetts Institute of Technology, Cambridge, MA 02139-4307; and <sup>e</sup>Department of Physics, University of Warwick, Coventry CV4 7AL, United Kingdom

Edited by Charles S. Peskin, New York University, New York, NY, and approved November 9, 2015 (received for review July 30, 2015)

Rheotaxis, the directed response to fluid velocity gradients, has been shown to facilitate stable upstream swimming of mammalian sperm cells along solid surfaces, suggesting a robust physical mechanism for long-distance navigation during fertilization. However, the dynamics by which a human sperm orients itself relative to an ambient flow is poorly understood. Here, we combine microfluidic experiments with mathematical modeling and 3D flagellar beat reconstruction to quantify the response of individual sperm cells in time-varying flow fields. Single-cell tracking reveals two kinematically distinct swimming states that entail opposite turning behaviors under flow reversal. We constrain an effective 2D model for the turning dynamics through systematic large-scale parameter scans, and find good quantitative agreement with experiments at different shear rates and viscosities. Using a 3D reconstruction algorithm to identify the flagellar beat patterns causing left or right turning, we present comprehensive 3D data demonstrating the rolling dynamics of freely swimming sperm cells around their longitudinal axis. Contrary to current beliefs, this 3D analysis uncovers ambidextrous flagellar waveforms and shows that the cell's turning direction is not defined by the rolling direction. Instead, the different rheotactic turning behaviors are linked to a broken mirror symmetry in the midpiece section, likely arising from a buckling instability. These results challenge current theoretical models of sperm locomotion.

sperm swimming | rheotaxis | fluid dynamics | microfluidics | simulations

Taxis, the directed kinematic response to external signals, is a defining feature of living things that affects their reproduction, foraging, migration, and survival strategies (1–4). Higher organisms rely on sophisticated networks of finely tuned sensory mechanisms to move efficiently in the presence of chemical or physical stimuli. However, various fundamental forms of taxis are already manifest at the unicellular level, ranging from chemotaxis in bacteria (5) and phototaxis in unicellular green algae (2) to the mechanical response (durotaxis) of fibroblasts (6) and rheotaxis (7, 8) in spermatozoa (3, 9–12). Over the last few decades, much progress has been made in deciphering chemotactic, phototactic, and durotactic pathways in prokaryotic and eukaryotic model systems. In contrast, comparatively little is known about the physical mechanisms that enable flow gradient sensing in sperm cells (3, 9–13). Recent studies (3, 12) suggest that mammalian sperm use rheotaxis for long-distance navigation, but it remains unclear how shear flows alter flagellar beat patterns in the vicinity of surfaces and, in particular, how such changes in the beat dynamics affect the steering process. Answering these questions will be essential for evaluating the importance of chemical (14) and physical (4) signals during mammalian fertilization (15–17).

A necessary requirement for any form of directed kinematic response is the ability to change the direction of locomotion. Multiflagellate bacteria achieve this feat by varying their motor activity, resulting in alternating phases of entangled and disentangled flagellar dynamics that give rise to run-and-tumble motion (5). A similar mechanism was recently discovered in the biflagellate eukaryote *Chlamydomonas reinhardtii* (18). This unicellular green alga actively redirects its swimming motion through occasional desynchronization of its two cilia (19), although it is still debated

whether this effect is of mechanical (20) or hydrodynamic (21, 22) origin. Experiments (23) show that the alga's reorientation dynamics can lead to localization in shear flow (24, 25), with potentially profound implications in marine ecology. In contrast to taxis in multiflagellate organisms (2, 5, 18, 26, 27), the navigation strategies of unflagellate cells are less well understood. For instance, it was discovered only recently that unflagellate marine bacteria, such as *Vibrio alginolyticus* and *Pseudoalteromonas haloplanktis*, use a buckling instability in their lone flagellum to change their swimming direction (28). However, as passive prokaryotic flagella differ fundamentally from their active eukaryotic counterparts, it is unclear to what extent such insights translate to spermatozoa.

Earlier studies of human sperm locomotion have identified several potential steering and transport mechanisms, including thermotaxis (4), uterine peristalsis (29, 30), and chemotaxis (14, 16, 31), but their relative importance has yet to be quantified. Recent experiments (3, 32, 33) demonstrate that rheotaxis, combined with steric surface alignment (12, 34), enables robust long-distance navigation by turning sperm cells preferentially against an externally imposed flow direction (9, 10), but how exactly this realignment process happens is unknown. It has been suggested (32, 35, 36) that the intrinsic curvature or chiral beat dynamics (37, 38) of the flagellum could play an essential role in rheotactic steering, but this remains to be confirmed in experiments. Similarly, an increasing number of theoretical models (36, 39–47) still await empirical validation, because 3D data for the beat pattern of sperm swimming close to surfaces has been lacking.

To examine the dynamics of human sperm rheotaxis quantitatively, we here combine microfluidic experiments with mathematical modeling and 3D flagellar beat reconstruction. Single-cell tracking

## Significance

Successful sperm navigation is essential for sexual reproduction, yet we still understand relatively little about how sperm cells are able to adapt their swimming motion in response to chemical and physical cues. This lack of knowledge is owed to the fact that it has been difficult to observe directly the full 3D dynamics of the whip-like flagellum that propels the cell through the fluid. To overcome this deficiency, we apply a new algorithm to reconstruct the 3D beat patterns of human sperm cells in experiments under varying flow conditions. Our analysis reveals that the swimming strokes of human sperm are considerably more complex than previously thought, and that sperm may use their heads as rudders to turn right or left.

Author contributions: A.B., I.K., N.S., J.D., and V.K. designed research; A.B., I.K., N.S., J.D., and V.K. performed research; A.B., I.K., N.S., J.D., and V.K. analyzed data; and N.S., J.D., and V.K. wrote the paper.

The authors declare no conflict of interest.

This article is a PNAS Direct Submission.

Freely available online through the PNAS open access option.

<sup>1</sup>A.B., I.K., and N.S. contributed equally.

<sup>2</sup>To whom correspondence should be addressed. Email: dunkel@math.mit.edu.

This article contains supporting information online at [www.pnas.org/lookup/suppl/doi:10.1073/pnas.1515159112/-DCSupplemental](http://www.pnas.org/lookup/suppl/doi:10.1073/pnas.1515159112/-DCSupplemental).

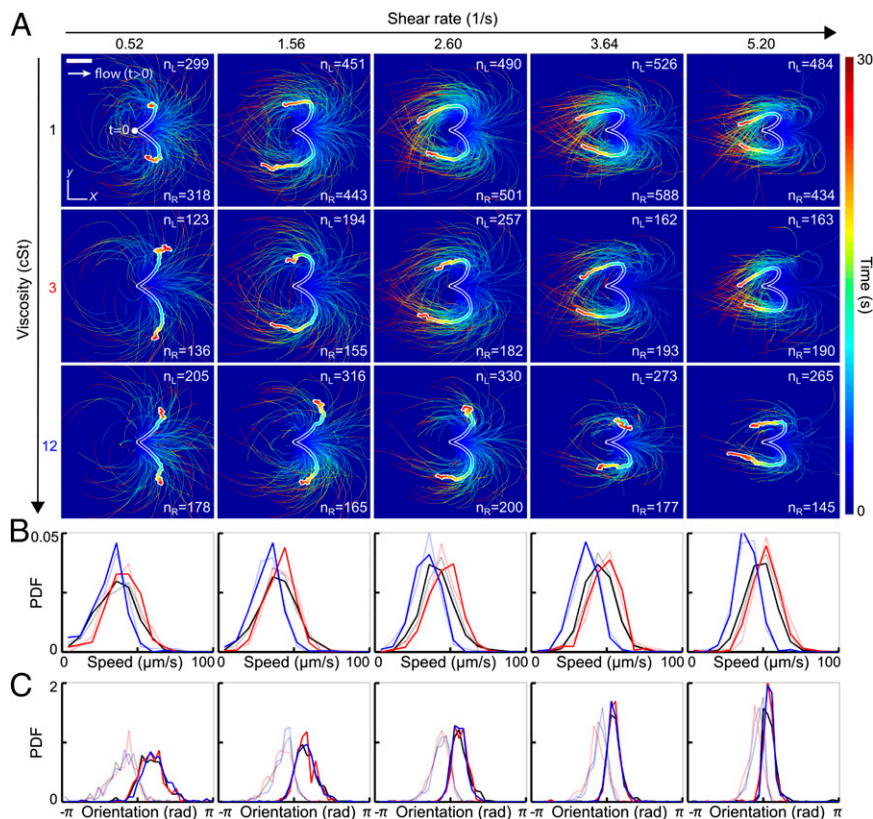


**Fig. 1.** Turning behavior of human sperm under flow reversal reveals two kinematically distinct swimming states. (A) Trajectories of individual sperm cells swimming close to the channel boundary in the  $(x, y)$  plane, with initial positions superimposed at time  $t = 0$  (viewed from inside the channel). Equal-time trajectory averages for left- and right-turning cells are shown as thick white-shaded lines. Flow was reversed at  $t = 0$ , pointing in positive  $x$  direction for  $t > 0$  (white arrow). The shear velocity increases linearly in  $z$  direction. Color encodes time. (Scale bar,  $200 \mu\text{m}$ .) (B) Normalized speed distributions before flow reversal at time  $t = 0$ . Faint lines indicate left-turning cells, and the other lines indicate right-turning cells. (C) Distribution of the orientation angles  $\varphi(0)$ , measured relative to the  $x$  axis before flow reversal at time  $t = 0$ , signals two kinematically distinct cell populations. Colors in B and C indicate different viscosities (black, 1 cSt; red, 3 cSt; blue, 12 cSt).

reveals the existence of two kinematically distinct swimming states that result in opposite turning behaviors under flow reversal. We quantify this effect for a range of viscosities and shear rates, and use these comprehensive data to constrain an effective 2D model through a systematic large-scale scan ( $>6,000$  parameter combinations). To identify the details of the flagellar beat dynamics during rheotaxis, we developed an algorithm that translates 2D intensity profiles into 3D positional data. Our 3D analysis confirms that human sperm perform a rolling motion (48), characterized by weakly nonplanar beat patterns and a rotating beat plane. However, contrary to current beliefs, we find that neither the rolling direction nor beat helicity determine the turning direction after flow reversal. Instead, the rheotactic turning behavior correlates with a previously unrecognized asymmetry in the midpiece, likely caused by a buckling instability. These findings call for a revision and extension of current models (36, 39–44, 46).

## Results

**Reorientation Dynamics After Flow Reversal.** Understanding how efficiently a sperm cell can react to directional changes in ambient fluid flows is a first step toward evaluating the importance of uterine peristalsis on sperm transport during reproduction (29, 30). To examine the response of human sperm after a sudden flow reversal, we tracked individual cells in microfluidic channels (*Experimental Details*) at three different kinematic viscosities  $\nu = 1$  centi-Stokes (cSt), 3 cSt, and 12 cSt, and five different shear rates,  $\dot{\gamma} = 0.52 \text{ s}^{-1}$ ,  $1.56 \text{ s}^{-1}$ ,  $2.60 \text{ s}^{-1}$ ,  $3.64 \text{ s}^{-1}$ , and  $5.20 \text{ s}^{-1}$  (Fig. 1). Hydrodynamic and steric forces cause sperm to accumulate near solid boundaries (12), where they remain trapped for several minutes while being exposed to a locally linear normal flow gradient. In our experiments, cells

generally accumulated at distances of  $<10 \mu\text{m}$  from the wall. We therefore fixed the focal plane parallel to the upper wall of the microfluidic chamber, using a large depth of field to track all cells within distance  $10 \mu\text{m}$  from the wall. The results presented below are thus integrated measurements over this accumulation layer. At time  $t < 0$ , a constant external flow field was applied in negative  $x$  direction, causing the cells to align preferentially in positive  $x$  direction (3, 32). At  $t = 0$ , the flow direction was rapidly reversed (switching time  $\lesssim 1 \text{ s}$ ), and the motions of 300 to 1,000 randomly selected sperm cells were tracked for a period of  $>30 \text{ s}$  for each parameter pair  $(\nu, \dot{\gamma})$ .

Trajectory analysis shows that approximately half of the tracked cells respond to flow reversal by making a right turn whereas the other half pursue a left turn (Fig. 1A and *Movies S1–S6*). In both cases, the majority of cells perform a complete U-turn, provided the shear rate is sufficiently large  $\dot{\gamma} > 1.56 \text{ s}^{-1}$ . As the value of  $\dot{\gamma}$  is increased, the characteristic curvature of the U-turns also increases, and the spread around the mean trajectories, obtained by averaging positions at equal time  $t > 0$ , is reduced (thick white-shaded lines in Fig. 1A).

The initial speed distributions, measured at the moment of the flow switch  $t = 0$ , show little variation between left-turning and right-turning cells (Fig. 1B). As expected, the maximum of the speed distribution is shifted to a lower value at high viscosity (blue curves in Fig. 1B). Strikingly, the initial offset angles  $\varphi(0)$  of left-turning and right-turning individuals are bimodally distributed, suggesting that exposure to constant flow for  $t < 0$  separates two different alignment modes that become magnified during a flow reversal (Fig. 1C).



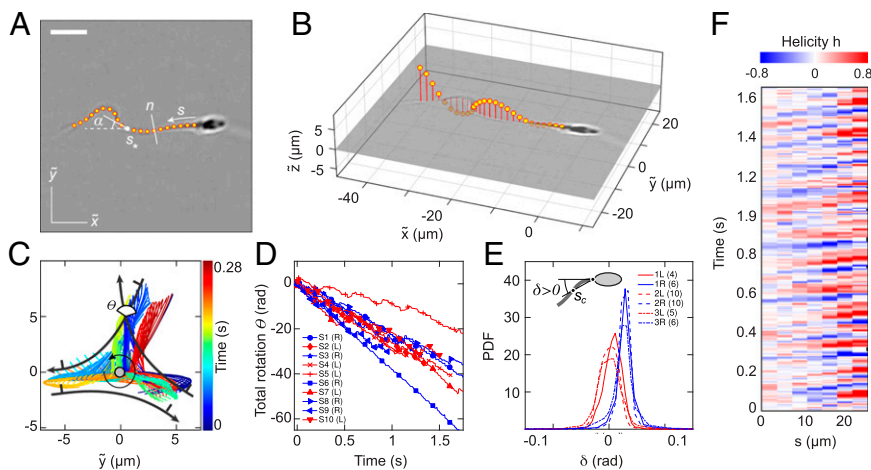


**Fig. 3.** A 3D flagellar beat reconstruction reveals that a mirror symmetry breaking in the midpiece curvature separates left-turning from right-turning sperm. (A) A 2D bright-field image and tracked flagellum in the head-centered comoving frame, with arc-length  $s$  and normal line  $n$ . (Scale bar, 10  $\mu\text{m}$ .) (B) A 3D beat reconstruction in the head-centered frame (*Beat Reconstruction* and *Movie S7*). (C) Typical 3D beat plane rotation for a single sperm, seen from head-on, with beat period of  $\sim 0.08$  s. The circular arrow indicates rolling direction of the flagellum. (D) The cumulative beat plane rotation  $\theta$ , shown for 10 typical samples of left-turning (L) and right-turning (R) cells, implies that the rolling and turning direction are not correlated. (E) Midpiece curvature, quantified by the bend angle  $\delta$  between the tangent at  $s=0$  and the secant through  $s_c \approx 4$   $\mu\text{m}$ , correlates strongly with the turning direction (three different donors, sample size in brackets). (F) A 3D reconstruction reveals ambidextrous helicity in the first  $\sim 70\%$  of the flagellum.

completes the second half in another plane. The beat envelope is not symmetric about the vertical axis, due to the presence of the wall, which is located below the cell in the body-centered frame (Fig. 3C). A large number of beats are performed parallel to the wall, reflecting inhibition of rolling by hydrodynamic and steric interactions between wall and flagellum, as also observed in previous experiments (48) and simulations (42).

We quantify the beat planarity through the length ratio  $P = |r_-|/|r_+|$  of the two minor axis vectors  $r_{\pm}$  of the flagellar inertial ellipsoid (Fig. S6). The shortest axis  $r_-$  is normal to the best-fit plane through the flagellum, and  $P=0$  for planar curves. We find that the flagellum remains mostly planar (Fig. S7), with a sample mean of  $\langle P \rangle \approx 0.2$ , in excellent agreement with estimates from previous 2D orthogonal measurements (35). Tracking a single point at arc length  $s \approx 15$   $\mu\text{m}$  from the head, we obtain flagelloid curves similar to those observed in head-fixed mouse spermatozoa (Fig. S5) (48) and recent hydrodynamic simulations (40), corroborating the accuracy of the 3D reconstruction.

**Turning Behavior Is Independent of Rolling.** To test if the rolling motion causes different turning directions, we track the normal vector  $\mathbf{n} = (\tilde{n}_x, \tilde{n}_y, \tilde{n}_z)$  of the best-fit plane through the flagellum in the head-centered frame (Fig. 3C). The projected orientation angle  $\theta(t) = \tan^{-1}(\tilde{n}_z/\tilde{n}_y)$  is found to undergo persistent clockwise rotation, interrupted by short periods of counterclockwise rotation (Fig. 3D). These results reconcile seemingly contradicting earlier reports of purely unidirectional (54) and bidirectional (35) rolling motion in human sperm. Importantly, however, our data show no correlation between rolling and rheotactic turning direction of the sperm cells (Fig. 3D).

**Turning Behavior Is Independent of Beat Chirality.** It has been suggested that the beat patterns of human sperm flagella resemble spirals of well-defined helicity (32, 35, 36). If true, then the different turning behaviors could be caused by a chiral mechanism. Even though helicoidal models of human sperm swimming are widely used in theoretical studies (32, 40, 46), the helicity of the beat patterns has never been measured directly in experiments. Using our 3D data, we can determine the local helicity of the flagellum shape  $\Gamma(s)$  at time  $t$  from the binormal vector  $\mathbf{b}(t, s) = \Gamma'(s) \times \Gamma''(s) / |\Gamma'(s) \times \Gamma''(s)|$ . In the head-centered frame, a helicoidal flagellum winding in counterclockwise direction when viewed from the front has local helicity  $h(t, s) = \mathbf{b}(t, s) \cdot \mathbf{e}_x > 0$ , whereas

$h(t, s) < 0$  if the winding is clockwise. Plotting  $h(t, s)$  along the flagellum as a function of time, we find no persistent helicity (Fig. 3F). Instead, the flagellar dynamics is dominated by helicity waves of either handedness (Fig. 3F). The mean helicity  $H(t) = \frac{1}{L} \int_0^L h(t, s) ds$  fluctuates around zero, showing no discernible difference between left-turning and right-turning sperm (Figs. S8–S10).

**Midpiece Asymmetry Determines Turning Direction.** The midpiece connecting head and flagellar tail of a human sperm cell is  $\sim 5$   $\mu\text{m}$  long, and its microstructure differs from that of the remaining flagellum (55). Our 3D data reveal that, unexpectedly, left-turning and right-turning sperm exhibit a notably different midpiece curvature. To quantify this effect, we measured the bend angle  $\delta$  between the tangent at  $s=0$  and the secant through  $s_c \approx 4$   $\mu\text{m}$ , and found that the bend angle distributions of left-turning cells are centered near zero, whereas right-turning cells exhibit a mean bend angle of  $\delta \approx 0.04$  rad for  $\nu = 1$  cSt and  $\dot{\gamma} = 2.56$   $\text{s}^{-1}$  (Fig. 3E and Fig. S11).

## Discussion

**Structure of the 2D Model.** The 2D trajectory data reveal two kinetically distinct swimming states, corresponding to  $\chi = \pm 1$  in Eqs. 1 and 2. More precisely, it is necessary to postulate an intrinsic preference for left turning ( $\chi = +1$ ) or right turning ( $\chi = -1$ ) in the effective 2D model because of the experimental observation that, after reversal of the flow direction, the majority of cells perform a complete U-turn (Fig. 1 and *Movies S1–S6*). To clarify this important detail, we may consider a hypothetical collection of cells without intrinsic turning preference, corresponding to  $\chi = 0$ . If the flow is along the negative  $x$  direction ( $\sigma = -1$ ), the only stable fixpoint of Eq. 2 is  $\varphi = 0$ , corresponding to exact alignment against the flow direction. If we further assume that the cell orientations are approximately symmetrically distributed around this fixed point, then, after a flow reversal from  $\sigma = -1$  to  $\sigma = +1$ , about 50% of the cells would turn left and right, respectively. However, each of those subpopulations would stop turning once they reach the new stable orientation fixed point  $\varphi = \pi$ . Thus, the resulting trajectory ensemble would trace out an open  $W$  shape instead of the experimentally observed “closed heart” shape (Fig. 1A).

**Ambidextrous Beat Helicity.** Our 3D analysis implies that neither rolling direction nor helicity controls the rheotactic turning



4. Bahat A, et al. (2003) Thermo taxis of mammalian sperm cells: A potential navigation mechanism in the female genital tract. *Nat Med* 9(2):149–150.
5. Berg HC, Brown DA (1972) Chemotaxis in *Escherichia coli* analysed by three-dimensional tracking. *Nature* 239(5374):500–504.
6. Lo CM, Wang HB, Dembo M, Wang YL (2000) Cell movement is guided by the rigidity of the substrate. *Biophys J* 79(1):144–152.
7. Pedley TJ, Kessler JO (1992) Hydrodynamic phenomena in suspensions of swimming microorganisms. *Annu Rev Fluid Mech* 24:313–358.
8. Marcos F, Fu HC, Powers TR, Stocker R (2012) Bacterial rheotaxis. *Proc Natl Acad Sci USA* 109(13):4780–4785.
9. Adolph H (1905) Die Spermatozoen der Säugetiere schwimmen gegen den Strom. *Anat Anz* 26(20-21):549–559.
10. Rothschild L (1963) Non-random distribution of bull spermatozoa in a drop of sperm suspension. *Nature* 198(4886):1221–1222.
11. Zimmer RK, Riffell JA (2011) Sperm chemotaxis, fluid shear, and the evolution of sexual reproduction. *Proc Natl Acad Sci USA* 108(32):13200–13205.
12. Kantsler V, Dunkel J, Polin M, Goldstein RE (2013) Ciliary contact interactions dominate surface scattering of swimming eukaryotes. *Proc Natl Acad Sci USA* 110(4):1187–1192.
13. Elgeti J, Winkler RG, Gompper G (2015) Physics of microswimmers—Single particle motion and collective behavior: A review. *Rep Prog Phys* 78(5):056601.
14. Brenker C, et al. (2012) The CatSper channel: A polymodal chemosensor in human sperm. *EMBO J* 31(7):1654–1665.
15. Eisenbach M, Gijalás LC (2006) Sperm guidance in mammals—An unpaved road to the egg. *Nat Rev Mol Cell Biol* 7(4):276–285.
16. Kaupp UB, Kashikar ND, Weyand I (2008) Mechanisms of sperm chemotaxis. *Annu Rev Physiol* 70:93–117.
17. Alvarez L, Friedrich BM, Gompper G, Kaupp UB (2014) The computational sperm cell. *Trends Cell Biol* 24(3):198–207.
18. Polin M, Tuval I, Drescher K, Gollub JP, Goldstein RE (2009) *Chlamydomonas* swims with two “gears” in a eukaryotic version of run-and-tumble locomotion. *Science* 325(5939):487–490.
19. Goldstein RE (2015) Green algae as model organisms for biological fluid dynamics. *Annu Rev Fluid Mech* 47:343–375.
20. Friedrich BM, Jülicher F (2012) Flagellar synchronization independent of hydrodynamic interactions. *Phys Rev Lett* 109(13):138102.
21. Goldstein RE, Polin M, Tuval I (2011) Emergence of synchronized beating during the regrowth of eukaryotic flagella. *Phys Rev Lett* 107(14):148103.
22. Brumley DR, Wan KY, Polin M, Goldstein RE (2014) Flagellar synchronization through direct hydrodynamic interactions. *eLife* 3:e02750.
23. Durham WM, Kessler JO, Roman S (2009) Disruption of vertical motility by phytoplankton layers. *Science* 323:1067–1070.
24. Zottl A, Stark H (2013) Periodic and quasiperiodic motion of an elongated microswimmer in Poiseuille flow. *Eur Phys J E Soft Matter* 36(1):4.
25. Rusconi R, Guasto JS, Stocker R (2014) Bacterial transport suppressed by fluid shear. *Nat Phys* 10:212–217.
26. Leptos KC, et al. (2013) Antiphase synchronization in a flagellar-dominance mutant of *Chlamydomonas*. *Phys Rev Lett* 111(15):158101.
27. Bennett RR, Golestanian R (2015) A steering mechanism for phototaxis in *Chlamydomonas*. *J R Soc Interface* 12(104):20141164.
28. Son K, Guasto JS, Stocker R (2013) Bacteria can exploit a flagellar buckling instability to change direction. *Nat Phys* 9:1–5.
29. Kunz G, Beil D, Deininger H, Wildt L, Leyendecker G (1996) The dynamics of rapid sperm transport through the female genital tract: Evidence from vaginal sonography of uterine peristalsis and hysterosalpingoscintigraphy. *Hum Reprod* 11(3):627–632.
30. Fauci LJ, Dillon R (2006) Biofluidmechanics of reproduction. *Annu Rev Fluid Mech* 38:371–394.
31. Spehr M, et al. (2003) Identification of a testicular odorant receptor mediating human sperm chemotaxis. *Science* 299(5615):2054–2058.
32. Kantsler V, Dunkel J, Blayney M, Goldstein RE (2014) Rheotaxis facilitates upstream navigation of mammalian sperm cells. *eLife* 3:02403.
33. Tung CK, et al. (2015) Emergence of upstream swimming via a hydrodynamic transition. *Phys Rev Lett* 114(10):108102.
34. Denissenko P, Kantsler V, Smith DJ, Kirkman-Brown J (2012) Human spermatozoa migration in microchannels reveals boundary-following navigation. *Proc Natl Acad Sci USA* 109(21):8007–8010.
35. Ishijima S, Hamaguchi MS, Naruse M, Ishijima SA, Hamaguchi Y (1992) Rotational movement of a spermatozoon around its long axis. *J Exp Biol* 163:15–31.
36. Smith DJ, Gaffney EA, Gadêlha H, Kapur N, Kirkman-Brown JC (2009) Bend propagation in the flagella of migrating human sperm, and its modulation by viscosity. *Cell Motil Cytoskeleton* 66(4):220–236.
37. Hilfinger A, Jülicher F (2008) The chirality of ciliary beats. *Phys Biol* 5(1):016003.
38. Friedrich BM, Riedel-Kruse IH, Howard J, Jülicher F (2010) High-precision tracking of sperm swimming fine structure provides strong test of resistive force theory. *J Exp Biol* 213(Pt 8):1226–1234.
39. Fauci LJ, McDonald A (1995) Sperm motility in the presence of boundaries. *Bull Math Biol* 57(5):679–699.
40. Smith DJ, Gaffney EA, Blake JR, Kirkman-Brown JC (2009) Human sperm accumulation near surfaces: A numerical study. *J Fluid Mech* 621:289–320.
41. Evans AA, Lauga E (2010) Propulsion by passive filaments and active flagella near boundaries. *Phys Rev E Stat Nonlin Soft Matter Phys* 82(4 Pt 1):041915.
42. Elgeti J, Kaupp UB, Gompper G (2010) Hydrodynamics of sperm cells near surfaces. *Biophys J* 99(4):1018–1026.
43. Gaffney EA, Gadelha H, Smith DJ, Blake JR, Kirkman-Brown JC (2011) Mammalian sperm motility: Observation and theory. *Annu Rev Fluid Mech* 43:501–528.
44. Montenegro-Johnson TD, Smith AA, Smith DJ, Loghin D, Blake JR (2012) Modelling the fluid mechanics of cilia and flagella in reproduction and development. *Eur Phys J E Soft Matter* 35(10):111.
45. Lauga E, Eloy C (2013) Shape of optimal active flagella. *J Fluid Mech* 730:R1.
46. Ishimoto K, Gaffney EA (2015) Fluid flow and sperm guidance: A simulation study of hydrodynamic sperm rheotaxis. *J R Soc Interface* 12(106):20150172.
47. Lauga E, Powers TR (2009) The hydrodynamics of swimming microorganisms. *Rep Prog Phys* 72:096601.
48. Woolley DM (2003) Motility of spermatozoa at surfaces. *Reproduction* 126(2):259–270.
49. Lee S-H, Grier DG (2007) Holographic microscopy of holographically trapped three-dimensional structures. *Opt Express* 15(4):1505–1512.
50. Wilson LG, Carter LM, Reece SE (2013) High-speed holographic microscopy of malaria parasites reveals ambidextrous flagellar waveforms. *Proc Natl Acad Sci USA* 110(47):18769–18774.
51. Wilson L, Zhang R (2012) 3D localization of weak scatterers in digital holographic microscopy using Rayleigh-Sommerfeld back-propagation. *Opt Express* 20(15):16735–16744.
52. Riedel-Kruse IH, Hilfinger A, Howard J, Jülicher F (2007) How molecular motors shape the flagellar beat. *HFSP J* 1(3):192–208.
53. Phillips DM (1972) Comparative analysis of mammalian sperm motility. *J Cell Biol* 53(2):561–573.
54. Linnet L (1979) Human spermatozoa: Unidirectional rotation of the tail as indicated by head-to-head agglutinates. *Arch Androl* 2(2):157–161.
55. Mundy AJ, Ryder TA, Edmonds DK (1995) Asthenozoospermia and the human sperm mid-piece. *Hum Reprod* 10(1):116–119.
56. Lindemann CB, Goltz JS (1988) Calcium regulation of flagellar curvature and swimming pattern in triton X-100-extracted rat sperm. *Cell Motil Cytoskeleton* 10(3):420–431.
57. Chang H, Suarez SS (2011) Two distinct  $Ca^{2+}$  signaling pathways modulate sperm flagellar beating patterns in mice. *Biol Reprod* 85(2):296–305.
58. Bedu-Addo K, et al. (2008) Mobilisation of stored calcium in the neck region of human sperm—A mechanism for regulation of flagellar activity. *Int J Dev Biol* 52(5-6):615–626.
59. Gadêlha H, Gaffney EA, Goriely A (2013) The counterbend phenomenon in flagellar axonemes and cross-linked filament bundles. *Proc Natl Acad Sci USA* 110(30):12180–12185.
60. Woolley DM, Vernon GG (2001) A study of helical and planar waves on sea urchin sperm flagella, with a theory of how they are generated. *J Exp Biol* 204(Pt 7):1333–1345.
61. Gadêlha H, Gaffney EA, Smith DJ, Kirkman-Brown JC (2010) Nonlinear instability in flagellar dynamics: A novel modulation mechanism in sperm migration? *J R Soc Interface* 7(53):1689–1697.
62. Lauga E, DiLuzio WR, Whitesides GM, Stone HA (2006) Swimming in circles: Motion of bacteria near solid boundaries. *Biophys J* 90(2):400–412.
63. Rodríguez JA, et al. (2009) Propulsion of African trypanosomes is driven by bihelical waves with alternating chirality separated by kinks. *Proc Natl Acad Sci USA* 106(46):19322–19327.
64. Herráez-Domínguez JV, Gil García de León F, Díez-Sales O, Herráez-Domínguez M (2005) Rheological characterization of two viscosity grades of methylcellulose: An approach to the modeling of the thixotropic behaviour. *Colloid Polym Sci* 284(1):86–91.
65. Aziz N, Fear S, Taylor C, Kingsland CR, Lewis-Jones DI (1998) Human sperm head morphometric distribution and its influence on human fertility. *Fertil Steril* 70(5):883–891.
66. Grubbs FE (1969) Procedures for detecting outlying observations in samples. *Technometrics* 11(1):1–21.
67. Carlson AE, et al. (2003) CatSper1 required for evoked  $Ca^{2+}$  entry and control of flagellar function in sperm. *Proc Natl Acad Sci USA* 100(25):14864–14868.
68. Werner S, Rink JC, Riedel-Kruse IH, Friedrich BM (2014) Shape mode analysis exposes movement patterns in biology: Flagella and flatworms as case studies. *PLoS One* 9(11):e113083.
69. Bergou M, Wardetzky M, Robinson S, Audoly B, Grinspun E (2008) Discrete elastic rods. *ACM Trans Graph* 27(3):63.